

A giant radio bridge connecting two galaxy clusters in Abell 1758

A. Botteon ¹, ¹★ R. J. van Weeren ¹, G. Brunetti ², F. de Gasperin ³, H. T. Intema ^{1,4}, E. Osinga ¹, G. Di Gennaro ¹, T. W. Shimwell ^{5,1}, A. Bonafede ^{6,2,3}, M. Brügger ³, R. Cassano ², V. Cuciti ³, D. Dallacasa ^{6,2}, F. Gastaldello ⁷, S. Mandal ¹, M. Rossetti ⁷ and H. J. A. Röttgering ¹

¹Leiden Observatory, Leiden University, PO Box 9513, NL-2300 RA Leiden, the Netherlands

²INAF – IRA, via P. Gobetti 101, I-40129 Bologna, Italy

³Hamburger Sternwarte, Universität Hamburg, Gojenbergsweg 112, D-21029 Hamburg, Germany

⁴International Centre for Radio Astronomy Research – Curtin University, GPO Box U1987, Perth, WA 6845, Australia

⁵ASTRON, the Netherlands Institute for Radio Astronomy, Postbus 2, NL-7990 AA Dwingeloo, the Netherlands

⁶Dipartimento di Fisica e Astronomia, Università di Bologna, via P. Gobetti 93/2, I-40129 Bologna, Italy

⁷IASF – Milano, INAF, Via A. Corti 12, I-20133 Milano, Italy

Accepted 2020 August 18. Received 2020 July 16; in original form 2020 August 12

ABSTRACT

Collisions between galaxy clusters dissipate enormous amounts of energy in the intracluster medium (ICM) through turbulence and shocks. In the process, Mpc-scale diffuse synchrotron emission in form of radio haloes and relics can form. However, little is known about the very early phase of the collision. We used deep radio observations from 53 MHz to 1.5 GHz to study the pre-merging galaxy clusters A1758N and A1758S that are ~ 2 Mpc apart. We confirm the presence of a giant bridge of radio emission connecting the two systems that was reported only tentatively in our earlier work. This is the second large-scale radio bridge observed to date in a cluster pair. The bridge is clearly visible in the LOFAR image at 144 MHz and tentatively detected at 53 MHz. Its mean radio emissivity is more than one order of magnitude lower than that of the radio haloes in A1758N and A1758S. Interestingly, the radio and X-ray emissions of the bridge are correlated. Our results indicate that non-thermal phenomena in the ICM can be generated also in the region of compressed gas in-between infalling systems.

Key words: radiation mechanisms: non-thermal – galaxies: clusters: individual: A1758 – galaxies: clusters: intracluster medium – galaxies: clusters: general – radio continuum: general.

1 INTRODUCTION

In the past two decades, the presence of diffuse and extended synchrotron sources with steep spectra ($\alpha > 1$, with $S_\nu \propto \nu^{-\alpha}$) in merging galaxy clusters has been confirmed by numerous radio observations (e.g. van Weeren et al. 2019, for a recent review). Radio haloes (in cluster centres) and radio relics (in cluster outskirts) are among the largest (\sim Mpc-scale) and most common sources associated with the intracluster medium (ICM). Their origin is likely related to the process of cluster formation, where part of the energy dissipated into the ICM by turbulence and shocks can be channelled into non-thermal components, namely relativistic particles and magnetic fields (e.g. Brunetti & Jones 2014, for a review).

Highly sensitive observations at low frequencies with LOw Frequency ARray (LOFAR) are providing many new insights into the study of non-thermal phenomena in galaxy clusters. Recently, Govoni et al. (2019) observed an ~ 3 Mpc radio bridge connecting the pre-merging system Abell 399-401 ($z = 0.07$), showing that detectable non-thermal emission can be generated on scales larger than that of clusters.

Abell 1758 (hereafter A1758, see Fig. 1) is a system located at $z = 0.279$ composed of two massive galaxy clusters separated by a projected distance of ~ 2 Mpc: A1758N (in the north, the most massive one) and A1758S (in the south). X-ray observations suggest that the two clusters are gravitationally bound but have not interacted yet, that is, they are in a pre-merging phase (David & Kempner 2004; Botteon et al. 2018; Schellenberger et al. 2019). In addition, complex cluster dynamics and multiple sub-substructures are observed both in A1758N and A1758S, indicating that each of the two clusters is undergoing its own merger (e.g. Monteiro-Oliveira et al. 2017). In Botteon et al. (2018), we used 144 MHz LOFAR observations to study the well-known radio halo in A1758N and also discovered a new radio halo and a candidate radio relic in A1758S. More importantly, at low resolution we found a hint (2σ) of a bridge of radio emission connecting the two clusters which required a further study with more sensitive observations.

In this Letter, we report the results of an extensive campaign of deep, multifrequency, radio observations of the radio bridge connecting the galaxy clusters in A1758. Here, we adopt a Lambda cold dark matter cosmology with $\Omega_\Lambda = 0.7$, $\Omega_m = 0.3$, and $H_0 = 70 \text{ km s}^{-1} \text{ Mpc}^{-1}$, in which 1 arcsec corresponds to 4.233 kpc at the cluster redshift ($z = 0.279$) and the luminosity distance is $D_L = 1428$ Mpc.

* E-mail: botteon@strw.leidenuniv.nl

2 OBSERVATIONS AND DATA REDUCTION

We observed A1758 with the LOFAR Low/High Band Antenna (LBA/HBA) arrays, the upgraded Giant Metrewave Radio Telescope (GMRT), and the Jansky Very Large Array (JVLA). Details of our observations are summarized in Table 1. The data reduction procedures for each data set are briefly described below. For all calibrated data sets, the final imaging has been performed using WSCLEAN v2.8 (Offringa et al. 2014) with multiscale multifrequency deconvolution (Offringa & Smirnov 2017).

2.1 LOFAR

In Botteon et al. (2018), we analysed the pointing closest to A1758 (offset by $\sim 1.1^\circ$) coming from the LOFAR Two-meter Sky Survey (LoTSS; Shimwell et al. 2017, 2019). For this work, we exploit follow-up observations with LOFAR LBA (39–78 MHz) and HBA (120–168 MHz) in combination with four LoTSS pointings that lay within 3° of A1758. For LBA, the target and calibrator were jointly observed for 8 h using the multibeam capability of LOFAR, while HBA observations followed the scheme of LoTSS, namely 8 h runs book-ended by 10 min scans on flux density calibrators. Each observation was analysed individually with the pipelines developed by the LOFAR Surveys Key Science Project team (PREFACTOR, de Gasperin et al. 2019; KILLMS, Tasse 2014; Smirnov & Tasse 2015; DDFACET, Tasse et al. 2018) to correct for direction-independent effects and to perform a first round of direction-dependent calibration of the entire LOFAR field of view before combination. The image quality towards A1758 was improved following the scheme that has been adopted in recent LOFAR HBA works (e.g. Botteon et al. 2019, 2020; van Weeren et al., in preparation), which consists of the subtraction of the sources outside the target region from the visibility data, phase-shifting to the centre of the region, and correcting the LOFAR station beam towards this direction. Residual artefacts are reduced by means of phase and amplitude self-calibration loops in the small region containing the target. The same procedure was adapted with optimized parameters for the LBA data. We set conservative systematic uncertainties of 15 per cent and 20 per cent on 53 MHz (LBA) and 144 MHz (HBA) flux densities, respectively.

2.2 uGMRT

We have observed A1758 for 20 h in band 3 (300–500 MHz) with the uGMRT. Data were recorded in 2048 frequency channels with integration time of 4 s in full Stokes mode. The data set was split into six frequency slices with a bandwidth of 33.3 MHz centred from 317 to 482 MHz that were processed independently using the SPAM pipeline (Intema et al. 2009). In the final analysis, we removed the highest frequency sub-band due to its lower quality and jointly deconvolved the remaining five slices to produce images with a central frequency at 383 MHz. The systematic uncertainty due to residual amplitude errors was set to 15 per cent.

2.3 JVLA

The JVLA *L*-band (1–2 GHz) observations consist of two 1.1 h runs performed with the C and D arrays. Each data set was reduced following standard procedures, including removal of the radio frequency interference, calibration of antenna delays and positions, bandpass, cross-hand delays, and polarization leakage and angle. To optimize the image quality, we performed various iterations of self-calibration to calculate the calibration solutions. First, three rounds of phase and

three rounds of amplitude calibrations are done on the C and D array data separately. Then, another six rounds of self-calibration were performed on the combined C + D array to produce the final data set with central frequency 1.5 GHz. The absolute flux scale calibration error was set to 5 per cent.

3 RESULTS

We produced deep images of the A1758 system using the observations listed in Table 1. Our LOFAR HBA image in Fig. 1 is a factor of ~ 2 deeper than that published in Botteon et al. (2018) as a result of the combination of different observations and recent improvements in the data reduction pipelines. In order to properly study the extended emission from the ICM and determine its flux density, a careful subtraction of the emission from discrete sources embedded in the cluster emission must be performed. For this reason, we followed the approach reported in Botteon et al. (2018), in which different models of point sources are subtracted from the visibilities to assess the accuracy of the procedure. Our discrete sources models were created by making six images with inner *uv*-cuts equally spaced in the range 1.0–3.5 $k\lambda$ (equivalent to 873–249 kpc at the redshift of A1758) for the LOFAR HBA and LBA, uGMRT and JVLA data sets deploying custom cleaning masks (e.g. Fig. 1). In this phase, multiscale cleaning was switched off to minimize the amount of diffuse emission from the ICM picked up by the deconvolution algorithm. The aforementioned models were subtracted individually from the visibilities and six images of the diffuse emission were produced with the same WSCLEAN parameters for each data set. An example of low-resolution images from 53 MHz to 1.5 GHz with comparable restoring beams are reported in Fig. 2. In the following, quoted flux densities at a given frequency represent the median value of the six different source-subtracted images measured in the same regions (the relative standard deviation of the six images is typically $\lesssim 2$ per cent).

The presence of diffuse radio sources in A1758N and A1758S is confirmed from 53 MHz to 1.5 GHz (Fig. 2). Most remarkably, we clearly observe a bridge of emission connecting the two clusters in the LOFAR image at 144 MHz, where the emission fills the region between A1758N and A1758S and has an integrated flux density of 24.2 ± 4.9 mJy. Low-significance patches of emission are observed both at 53 and 383 MHz, the most significant of which is a filamentary structure extending from the halo in A1758N towards A1758S detected above the 3σ level at 53 MHz. This region is encompassed by the white box shown in Fig. 2 (top-left panel) where we measure flux densities of $S_{53\text{MHz}} = 60.2 \pm 10.7$ and $S_{144\text{MHz}} = 11.6 \pm 2.4$ mJy, leading to $\alpha = 1.65 \pm 0.27$. By assuming a limit at 3σ on the 53 MHz flux density, the average spectral index on the entire bridge results $\alpha < 1.84$, while current uGMRT and JVLA data provide only a loose constraint of $\alpha > 0.4$.

The flux densities and integrated spectra of the other diffuse sources in the system measured from the red regions shown in Fig. 1 (which were drawn to roughly follow the 3σ level contour of the LOFAR HBA image in Fig. 2) are reported in Fig. 3. Our measurements agree with the results of Botteon et al. (2018) and Schellenberger et al. (2019).

4 DISCUSSION

Radio bridges connecting pre-merging clusters are a recent discovery. So far, the cluster pairs A1758N–A1758S (at $z = 0.279$) and Abell 399–401 (at $z = 0.07$, Govoni et al. 2019) are the only two cases where a bridge of radio emission between two clusters has been observed.

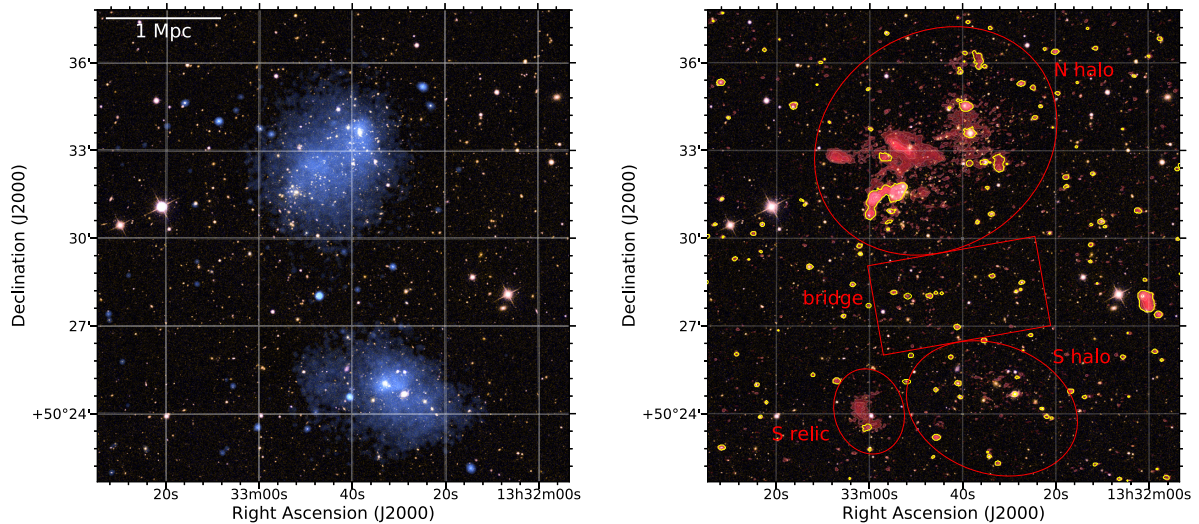


Figure 1. Composite images of A1758 obtained from the superposition of an optical SDSS g, r, i mosaic with *Chandra* (blue) and with a LOFAR image at 144 MHz with a resolution of $7.6 \text{ arcsec} \times 5.4 \text{ arcsec}$ (red) and a rms noise of $60 \mu\text{Jy beam}^{-1}$. Yellow and red regions indicate the mask used to subtract discrete sources and the regions adopted to measure the flux densities in the low-resolution images, respectively.

Table 1. Radio observations used in this work. The offsets of A1758 from LoTSS pointing centres are: $^a 1.10^\circ$, $^b 1.70^\circ$, $^c 2.07^\circ$, and $^d 2.79^\circ$.

Telescope	Project	Observation date	Duration	Frequency band	Configuration	
LOFAR	LoTSS	LC12.006	2020-02-25	8 h	39–78 MHz	LBA Outer
		LC12.006	2019-09-29	8 h	120–168 MHz	HBA Dual Inner
		P42Hetdex07 ^a	2014-06-01	8 h	120–168 MHz	HBA Dual Inner
		P5Hetdex41 ^b	2014-07-28	8 h	120–168 MHz	HBA Dual Inner
		P38Hetdex07 ^c	2014-06-01	8 h	120–168 MHz	HBA Dual Inner
		P206 + 52 ^d	2015-04-28	8 h	120–168 MHz	HBA Dual Inner
uGMRT	37_030	2019-02-17/18	20 h	300–500 MHz	Band 3	
JVLA	18A-172	2018-09-17/20	1.1 h	1–2 GHz	L-band D-array	
	18A-172	2019-01-18/19	1.1 h	1–2 GHz	L-band C-array	

The two systems show remarkable similarities. First of all, each of the two main components of the pairs is a massive cluster, with $M_{500} \gtrsim 5 \times 10^{14} M_\odot$ (Planck Collaboration XXVII 2016). Secondly, both are pairs of dynamically disturbed clusters, with all four clusters undergoing mergers and hosting a radio halo (Murgia et al. 2010; Botteon et al. 2018). Conversely, recent LOFAR HBA observations failed to detect a radio bridge connecting the two clusters in the Lyra complex (Botteon et al. 2019), which are less massive and in that case only one of the two is a merging system/hosts a radio halo. This may suggest that radio bridges form from the dissipation of energy in dynamically active regions.

According to Brunetti & Vazza (2020), radio bridges may originate from second-order Fermi acceleration of electrons interacting with turbulent motions triggered by the complex dynamics in the overdense region between pre-merging clusters. The observation of infalling sub-groups on to A1758 (Haines et al. 2018; Schellenberger et al. 2019) would be in agreement with this scenario. One of the key predictions of this model is that the emission in radio bridges is volume-filling especially at low frequencies. In this respect, the detection at 144 MHz combined with the X-ray observations provides important information. In Fig. 4, we compare the X-ray and radio surface brightness of the bridge extracted in 31 regions and along 4 transverse slices, finding a remarkably good correlation between the two. We observe fluctuations of similar magnitude and morphology in radio and X-rays, suggesting that thermal and non-thermal emissions

are connected and originate from similar volumes. This connection is studied for the first time in a radio bridge and is in line with theoretical expectations. The spectrum of radio bridges also provides important information on their origin. Unfortunately, we were able to provide a spectral constraint only in a small region of the bridge, which may be not representative of the overall spectrum of the emission. Deeper observations are required for this kind of study. Based on the red regions in Fig. 1, we assume oblate spheroid geometries for the haloes and a cylindrical volume for the bridge to compute the average radio emissivity of the diffuse sources. The mean radio emissivity of the bridge is $\langle \epsilon \rangle_{144 \text{ MHz}} = 4.02 \times 10^{-43} \text{ erg s}^{-1} \text{ Hz}^{-1} \text{ cm}^{-3}$, that is more than one order of magnitude lower than that of the two haloes. We note that the emissivity of the bridge in A1758 is also similar (a factor of 2 lower) to that reported for the bridge in Abell 399-401 (Govoni et al. 2019), marking another similarity between the two pairs.

Regions between clusters give us the possibility to study the most diluted regions of the ICM that are accessible with current instruments (Vazza et al. 2019). They are dynamically very young, i.e. their dynamical age is comparable to the eddy turnover time of the turbulent eddies generated in these environments. Under these conditions, the media are characterized by a ratio of thermal to magnetic pressures reasonably > 100 (in clusters we believe that $P_{\text{th}}/P_B = 10\text{--}100$), providing unique laboratories to study magnetic

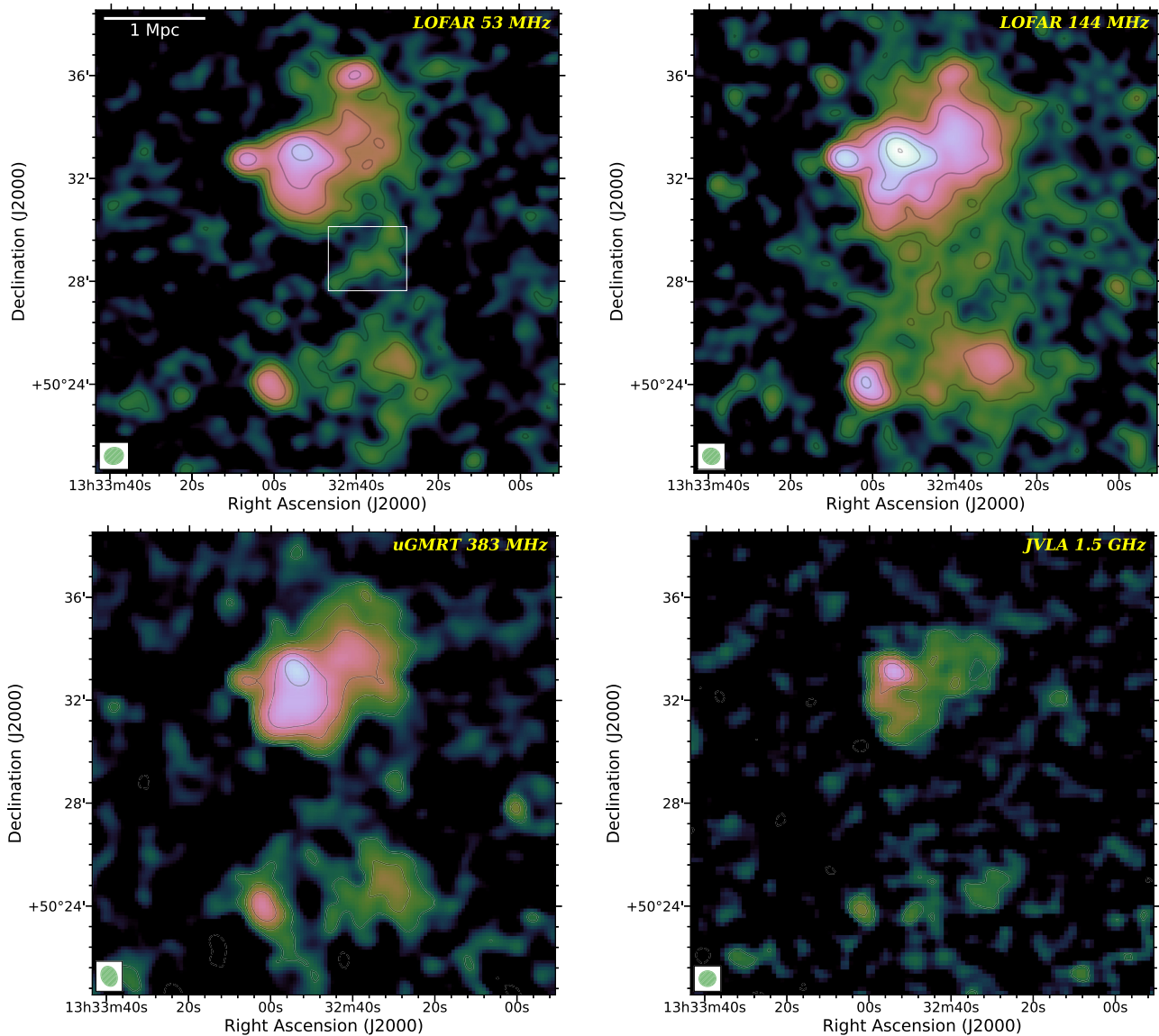


Figure 2. Radio images from 53 MHz to 1.5 GHz of A1758 with discrete sources subtracted. The colour scale has a logarithmic stretch from 0.5 to 200σ . Contours are drawn from 3σ and are spaced by a factor of 2, where $\sigma_{53\text{MHz}} = 1.6 \text{ mJy beam}^{-1}$, $\sigma_{144\text{MHz}} = 160 \text{ } \mu\text{Jy beam}^{-1}$, $\sigma_{383\text{MHz}} = 170 \text{ } \mu\text{Jy beam}^{-1}$, and $\sigma_{1.5\text{GHz}} = 80 \text{ } \mu\text{Jy beam}^{-1}$. Images were obtained by applying a Gaussian uv -taper of 35 arcsec; restoring beams are shown in the bottom left corners. The white box denotes the region where we measured a spectral index of $\alpha = 1.65 \pm 0.27$ between 53 and 144 MHz.

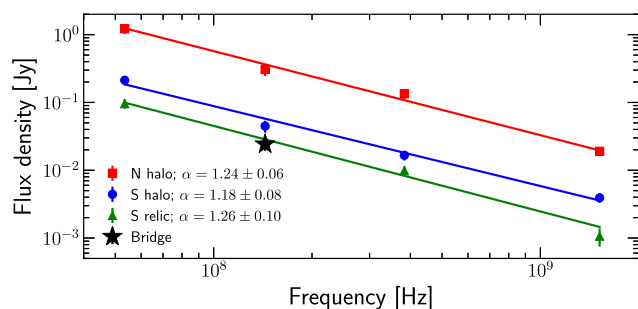


Figure 3. Integrated spectra of the diffuse radio sources.

field amplification and particle acceleration in new regimes (see Brunetti & Vazza 2020).

5 CONCLUSIONS

We have confirmed the presence of an ~ 2 Mpc radio bridge connecting the two galaxy clusters in A1758. A standalone detection could be claimed only at 144 MHz, where the radio and X-ray emissions are correlated, suggesting that they share similar emitting volumes. Only hints of radio emission are observed at 53 and 383 MHz, making uncertain the determination of its spectral index; deeper observations are required to provide a robust estimate of its value.

Only two giant intracluster radio bridges have been detected to date. These are among the most giant structures observed in the Universe so far, and their origin is likely related to the turbulence (and shocks) generated in the ICM during the initial stage of the merger, which boost both the radio and X-ray emission between the clusters. These detections demonstrate the existence of non-thermal components at large distances from cluster centres with

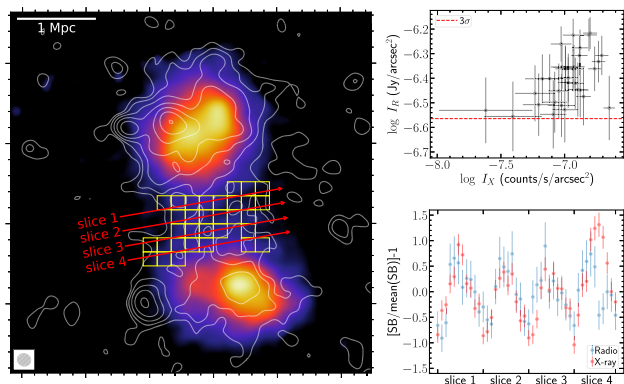


Figure 4. *Chandra* smoothed image in the 0.5–2.0 keV band overlaid with the low-resolution LOFAR HBA contours (left). The boxes and slices indicate the regions where the X-ray and radio surface brightness have been evaluated and compared (right).

important implications for the models of magnetic field amplification and particle acceleration in the most diluted regions of the ICM.

ACKNOWLEDGEMENTS

ABot, RJvW, and EO acknowledge support from the VIDI research programme with project number 639.042.729, which is financed by the Netherlands Organisation for Scientific Research (NWO). GDG acknowledges support from the ERC Starting Grant ClusterWeb 804208. ABon acknowledges support from the ERC-Stg DRANOEL n. 714245 and from the MIUR FARE grant ‘SMS’. GB, RC, FG, and MR acknowledge support from INAF mainstream project ‘Galaxy Clusters Science with LOFAR’ 1.05.01.86.05. VC acknowledges support from the Alexander von Humboldt Foundation. LOFAR (van Haarlem et al. 2013) is the Low Frequency Array designed and constructed by ASTRON. It has observing, data processing, and data storage facilities in several countries, which are owned by various parties (each with their own funding sources), and that are collectively operated by the ILT foundation under a joint scientific policy. The ILT resources have benefited from the following recent major funding sources: INSU-CNRS, Observatoire de Paris and Université d’Orléans, France; BMBF, MIWF-NRW, MPG, Germany; Science Foundation Ireland (SFI), Department of Business, Enterprise and Innovation (DBEI), Ireland; NWO, the Netherlands; The Science and Technology Facilities Council, UK; Ministry of Science and Higher Education, Poland; The Istituto Nazionale di Astrofisica (INAF), Italy. This research made use of the Dutch national e-infrastructure with support of the SURF Cooperative (e-infra 180169) and the LOFAR e-infra group. The Jülich LOFAR Long Term Archive and the German LOFAR network are both coordinated and operated by the Jülich Supercomputing Centre (JSC), and computing resources on the supercomputer JUWELS at JSC were provided by the Gauss Centre for Supercomputing e.V. (grant CHTB00) through the John

von Neumann Institute for Computing (NIC). This research made use of the University of Hertfordshire high-performance computing facility and the LOFAR-UK computing facility located at the University of Hertfordshire and supported by STFC [ST/P000096/1], and of the Italian LOFAR IT computing infrastructure supported and operated by INAF, and by the Physics Department of Turin University (under an agreement with Consorzio Interuniversitario per la Fisica Spaziale) at the C3S Supercomputing Centre, Italy. We thank the staff of the GMRT for support. GMRT is run by the National Centre for Radio Astrophysics of the Tata Institute of Fundamental Research. The NRAO is a facility of the National Science Foundation operated under cooperative agreement by Associated Universities, Inc.

DATA AVAILABILITY

The data underlying this article will be shared on reasonable request to the corresponding author.

REFERENCES

- Botteon A. et al., 2018, *MNRAS*, 478, 885
 Botteon A. et al., 2019, *A&A*, 630, A77
 Botteon A. et al., 2020, *ApJ*, 897, 93
 Brunetti G., Jones T., 2014, *IJMPD*, 23, 30007
 Brunetti G., Vazza F., 2020, *Phys. Rev. Lett.*, 124, 51101
 David L., Kempner J., 2004, *ApJ*, 613, 831
 de Gasperin F. et al., 2019, *A&A*, 622, A5
 Govoni F. et al., 2019, *Science*, 364, 981
 Haines C. et al., 2018, *MNRAS*, 477, 4931
 Intema H., van der Tol S., Cotton W., Cohen A., van Bemmel I., Röttgering H., 2009, *A&A*, 501, 1185
 Monteiro-Oliveira R., Cypriano E., Machado R., Lima Neto G., Ribeiro A., Sodré L., Dupke R., 2017, *MNRAS*, 466, 2614
 Murgia M., Govoni F., Feretti L., Giovannini G., 2010, *A&A*, 509, A86
 Offringa A., Smirnov O., 2017, *MNRAS*, 471, 301
 Offringa A. et al., 2014, *MNRAS*, 444, 606
 Planck Collaboration XXVII, 2016, *A&A*, 594, A27
 Schellenberger G., David L., O’Sullivan E., Vrtilek J., Haines C., 2019, *ApJ*, 882, 59
 Shimwell T. W., 2017, *A&A*, 104, 6361
 Shimwell T. W. et al., 2019, *A&A*, 622, A1
 Smirnov O., Tasse C., 2015, *MNRAS*, 449, 2668
 Tasse C., 2014, preprint ([arXiv:1410.8706](https://arxiv.org/abs/1410.8706))
 Tasse C. et al., 2018, *A&A*, 611, A87
 van Haarlem M. et al., 2013, *A&A*, 556, A2
 van Weeren R., de Gasperin F., Akamatsu H., Brüggén M., Feretti L., Kang H., Stroe A., Zandanel F., 2019, *Space Sci. Rev.*, 215, 16
 Vazza F., Etori S., Roncarelli M., Angelinelli M., Brüggén M., Gheller C., 2019, *A&A*, 627, A5

This paper has been typeset from a $\text{\TeX}/\text{\LaTeX}$ file prepared by the author.